

Modeling of macrosegregation in steel ingot: influence of mold shape and melt superheat

D. R. Liu^{1,2*}, X. H. Kang¹, P. X. Fu¹, D. Z. Li¹

¹*Institute of Metal Research, Chinese Academy of Science,
No. 72 Wen Hua Road, Shen He District, Shenyang 110016, China*

²*School of Materials Science and Engineering, Harbin University of Science and Technology,
No. 4 Lin Yuan Road, Xiang-Fang District, Harbin 150040, China*

Received 4 May 2010, received in revised form 26 July 2010, accepted 19 August 2010

Abstract

A continuum model for the transport phenomena in solidification systems is used to investigate the formation mechanism of macrosegregation in a 3.3 t steel ingot. Numerical scheme with explicit time stepping in solidification problems is developed for solving coupled temperature and concentration fields, and equations of momentum. Experimental measurements and numerical results in the literature are used as indications of the validity of present prediction. Influences of the mold shape and the melt superheat upon macrosegregation are investigated. Results show that for ingots with the same weight, reducing the size of hot top favors a pronounced positive-negative-positive concentration distribution along the centerline. A-segregates and positive-negative-positive concentration distribution are not found in the ingot with a modified hot top that has a more uniform section area. Higher superheat reduces the height of bottom negative segregation cone. For cases with superheat larger than zero, positively segregated patches are observed at the ingot bottom.

Key words: macrosegregation, steel ingot, mold shape, melt superheat

Nomenclature

C	– mixture concentration	C_{ref}	– reference concentration
$C_l / \langle C_s \rangle$	– liquid/average solid concentration	c_p	– specific heat
d_s	– mean grain diameter	f_s	– solid fraction
g	– gravity acceleration	H	– enthalpy
ΔH	– latent heat	K_o	– permeability coefficient
m_l	– slope of liquidus line	P	– pressure
T	– temperature	T_{ref}	– reference temperature
\vec{U}	– velocity vector	V, W	– x and y components of \vec{U}
v_l	– actual liquid velocity	β_C	– solutal expansion coefficient
β_T	– thermal expansion coefficient	ρ	– density
λ	– heat conductivity	μ_l	– viscosity of liquid

1. Introduction

Macrosegregation is one of classical problems in the field of solidification and casting, especially for large-scale ingots [1]. It is caused by the re-organization of chemical elements over larger distances than the dendrite arm spacing. The segregation patterns commonly

found in a steel ingot are top positive segregation zone and bottom negative segregation cone. Whether A-segregates can be observed or not depends upon the steel grade and the size and the shape of ingot [2]. These inhomogeneities, if occur, are unfortunately a permanent feature. They cause serious problems in the final steel properties and threaten the serviceab-

*Corresponding author: tel.: 024-23971429; e-mail address: nacylake@126.com

ility of the casting [1, 3]. Therefore, how to efficiently control macrosegregation during casting process depends greatly on a better understanding of its formation mechanism.

With several decades of intensive research, the reason for macrosegregation formation is qualitatively understood. Based on the well-established knowledge, one of the main goals of computer modeling is to quantitatively clarify the influences of processing and design parameters on the concentration distribution, because it is very vital for controlling or eliminating macrosegregation. Schneider et al. [4] numerically compared the segregation pattern of a ten-element steel alloy (E10) with that of binary Fe-C alloy (E2), and found a slightly more severe carbon segregation for E2 than E10. Much attention has been given to studying thermosolutal convection and resultant macrosegregation in irregular geometries by Rady et al. [5]. Calculated results show that a higher extent of segregation is found in ingots with positive or negative slopes compared to the rectangular ingot. Lee et al. [6] examined the effects of cooling rate and strength of gravity on the segregation formation. More homogeneous compositions are obtained for larger solidification rate and smaller gravity force. Combeau et al. [2] systematically studied the influences of motion and morphology of equiaxed grains on macrosegregation. Free-floating-dendritic-grain case presents a similar segregation tendency to the fixed-solid case. However, if the morphology of equiaxed grain is changed from dendritic to globular, a totally different segregation pattern is created, characterized as serious bottom negative segregation and pronounced top positive segregation. Moreover, A-segregates are not formed. Yadav et al. [7] considered the impact of filling process. For a small size casting, the filling course should not be neglected, since the residual flow after it significantly affects the shape of mush and hence, the segregation distribution.

Although the above mentioned numerical studies could help us to obtain a good understanding of macrosegregation formation under different conditions, some special phenomena occurred in the real casting process are still not explained. For example, authors' recent experimental measurement of 5 t sand-mold cast ingot showed a small positive segregation zone at the bottom of ingot, despite a negative segregation cone is usually expected. This phenomenon is numerically studied and clarified in the present work. Mold shape plays an important role and its influence upon macrosegregation formation deserves an investigation.

In this paper, a continuum model for the transport phenomena during solidification is used to perform the numerical studies. A time-explicit scheme is developed for solving the coupled temperature and concentration fields, and the equations of momentum. Self-developed scheme is verified by reproducing the data both in the

literature and in the experiment. Effects of mold shape and melt superheat on concentration distribution are examined. Mechanisms of the macrosegregation formation under different casting conditions are revealed.

2. Mathematical model

Mathematical model used is similar to the one proposed by Voller et al. [9, 10]. Before calculation, some assumptions are made:

1. laminar and Newtonian flow in the liquid phase,
2. two-dimensional calculations are carried out,
3. solid is considered to be rigid and stationary,
4. thermodynamic equilibrium at the solid-liquid interface,
5. liquid is assumed to fill the mold cavity simultaneously.

The last assumption is due to the fact that for a large-size ingot, the extent of solidification may be small during filling course. Since a significant cooling and solidification are avoided before filling is completed, the impact of mold-filling upon macrosegregation is not taken into account.

On the basis of these hypotheses, mass, momentum, mixture energy and mixture solute conservations are given. Although these equations can be found in [9, 10], they are still described for the intact of the paper.

Continuity:

$$\nabla \cdot (\vec{U}) = 0, \quad (1)$$

$$\vec{U} = (1 - f_s)v_1. \quad (2)$$

V-momentum:

$$\frac{\partial}{\partial t} (\rho V) + \nabla \cdot (\rho \vec{U} V) = -\frac{\partial P}{\partial x} - KV + \nabla \cdot (\mu_1 \nabla V). \quad (3)$$

W-momentum:

$$\begin{aligned} \frac{\partial}{\partial t} (\rho W) + \nabla \cdot (\rho \vec{U} W) = & -\frac{\partial P}{\partial y} - KW + \\ & + \nabla \cdot (\mu_1 \nabla W) + \rho g [\beta_T (T - T_{\text{ref}}) + \beta_C (C_1 - C_{\text{ref}})]. \end{aligned} \quad (4)$$

The mushy region is modeled by Carman-Kozeny relationship, where the parameter K is defined as:

$$K = \frac{K_o f_s^2}{(1 - f_s)^3}. \quad (5)$$

The permeability coefficient K_o is given as follows:

$$K_o = \frac{180 \times \mu_1}{d_s^2}. \quad (6)$$

Mixture energy conservation equation:

$$\frac{\partial}{\partial t}(\rho H) + \nabla \cdot (\rho c_p \vec{U} T + \rho \vec{U} \Delta H) = \lambda \nabla \cdot (\nabla T), \quad (7)$$

$$[\rho H] = f_s \rho_s c_p T + (1 - f_s) \rho_l c_p T + (1 - f_s) \rho_l \Delta H. \quad (8)$$

Mixture solute conservation equation:

$$\frac{\partial}{\partial t}[\rho C] + \nabla \cdot (\rho \vec{U} C_1) = 0, \quad (9)$$

$$[\rho C] = f_s \rho_s \langle C_s \rangle + (1 - f_s) \rho_l C_1. \quad (10)$$

During primary solidification the temperature and liquid concentration are related through the liquidus line:

$$T = T_m + m_1 C_1. \quad (11)$$

Temperature-concentration coupling is solved using the time-explicit scheme. Flow equations are dealt with by the Solution Algorithm for transient fluid flow (SOLA) technique, rather than the well-known time-implicit SIMPLER algorithm.

A certain solidification path is not pre-determined, indicating the finish of solidification is not judged by the solidus temperature. A similar method to that in [1] is employed. Solid fraction calculated by local temperature and concentration at each point is used as the criterion.

3. Validation of developed scheme

3.1. Numerical test

With the same assumptions, boundary conditions and input parameters, validation of code is carried out by comparing present calculated results with numerical results available in [2] that were both theoretically and experimentally verified. The modeled ingot (Fe-0.36wt.%C alloy, 3.3 t) is shown in Fig. 1. A refined mesh size $0.6 \times 0.6 \text{ cm}^2$ is selected in this paper, which is smaller than $0.7 \times 1.2 \text{ cm}^2$ in [2]. Time step is not larger than 0.01 s.

The major uncertainty in the literature is that thermal physical properties of hot top (refractory material and exothermic powder) are not given. Therefore, according to the same trials and previous experience of authors, properties in Table 1 are hired for the hot top in this study.

Figure 2 compares the present segregation ratio map with the existing numerical simulation. As observed in Figs. 2a,b, segregation characteristics in [2] are nearly all included in this study, including top positive segregation, bottom negative segregation cone, and A-segregation bands. For the clarity of presentation, Fig. 2b is simplified to Fig. 2c, according to

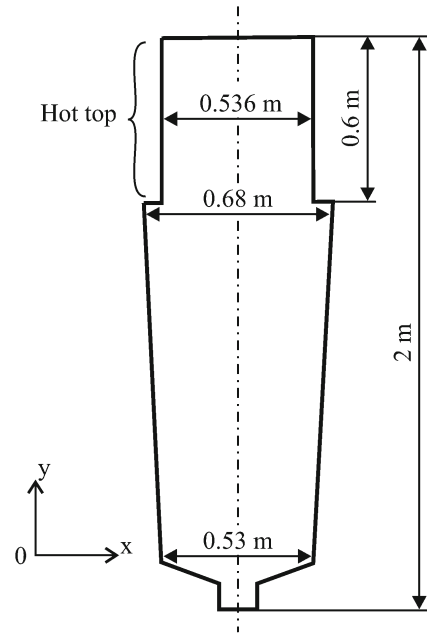


Fig. 1. Schematic diagram of 3.3 t ingot [2].

Table 1. Thermo-physical properties of hot top

	Refractory material	Exothermic powder
ρ_s (kg m^{-3})	500.0	210.0
λ ($\text{W m}^{-1} \text{K}^{-1}$)	0.9	0.9
c_p ($\text{J kg}^{-1} \text{K}^{-1}$)	600.0	1130.0

the segregation ratio range. It can be noted that the positive segregation patches near the ingot surfaces (Fig. 2a) are reproduced in Fig. 2b. For Fig. 2a, one thing should be mentioned. The bottom bar holder and a large part of hot top are not displayed in the picture. That is why Fig. 2b seems a little “taller” than Fig. 2a.

Figure 3 offers the distribution of carbon segregation ratio along centerline. The present prediction shows a fair agreement with that in [2], except the degree of positive segregation below the hot top is smaller, and positive segregation in the hot top is more serious. Such discrepancies may be contributed to the following factors: (i) different mathematical equations and numerical implementations are developed; (ii) different thermal physical parameters of hot top are selected. Despite these discrepancies, the test of present scheme with an acceptable outcome gives us confidence that the self-developed code is reasonable.

For the following study, the ingot in Fig. 1 is referred to base case.

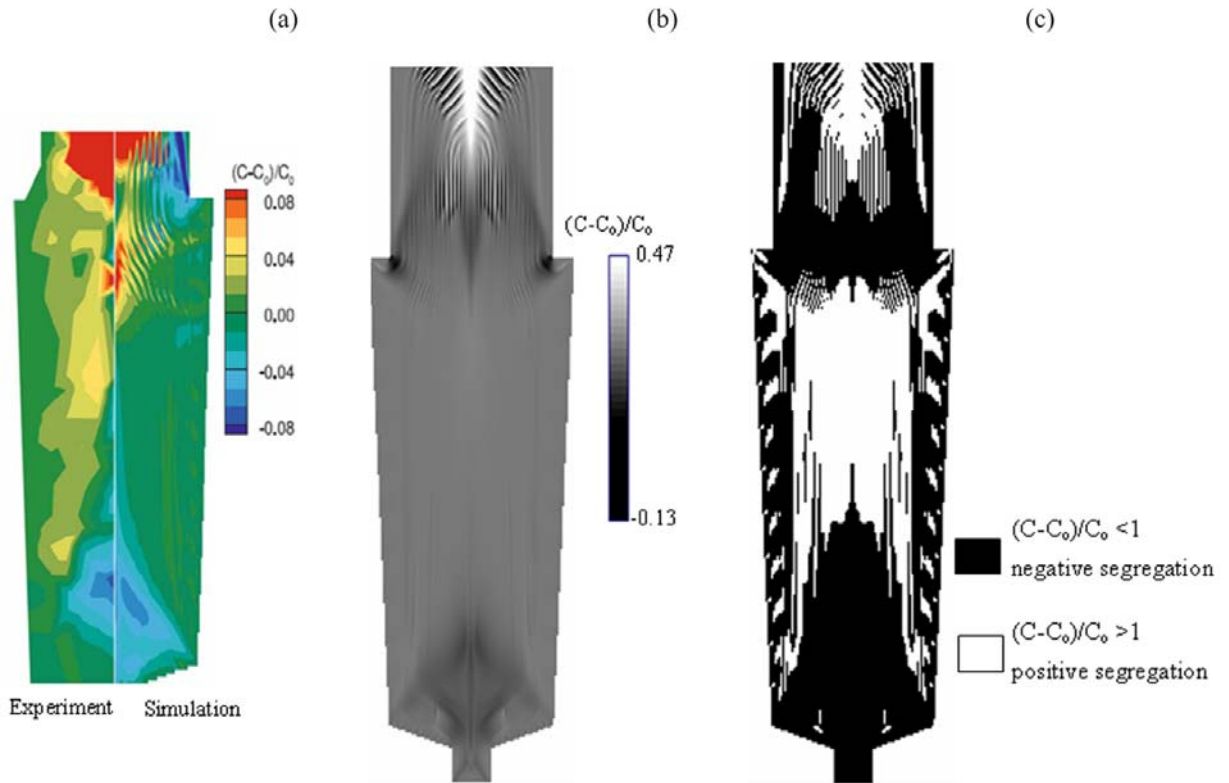


Fig. 2. Comparison of segregation ratio map: (a) result in [2], (b) present simulation, (c) simplified form of picture (b).

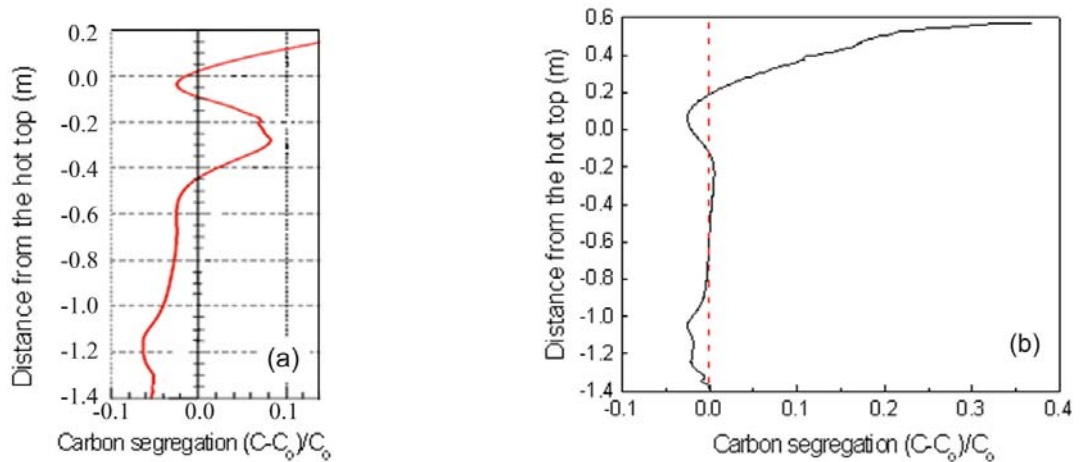


Fig. 3. Comparison of carbon segregation ratio distribution along centerline: (a) result in [2], (b) present simulation.

3.2. Experimental validation

To further establish the validity of the developed scheme, simulated results are compared to the experimental data.

A 5 t ingot was sand-mold cast by Institute of Metal Research, China [8]. The dimensions of ingot are shown in Fig. 4. The steel grade is reported in Table 2. The pouring temperature was 1552 °C with superheat 60 °C. The ingot was poured from the bottom and the mold filling time was about 180 s. The

Table 2. Steel grade of the 5 t ingot (wt.%)

C	Si	Mn	S	P	Fe
0.49	0.23	0.51	0.03	0.03	balance

top insulator consisted of a 10 cm thick layer of exothermic powder.

This practically-cast ingot was modeled. Selections of boundary condition and input parameters are sim-

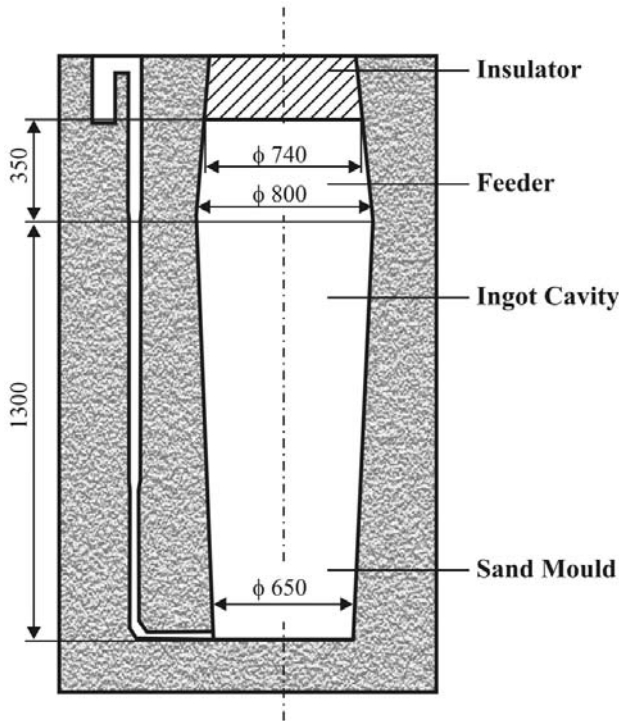


Fig. 4. Schematic diagram of experimental 5 t ingot.

ilar to those in [8]. Comparison between the sulfur-print of the experimental ingot and numerical prediction is shown in Fig. 5. For the sulfur-print, dark color corresponds to positive segregation, and light color corresponds to negative segregation. Some black discontinuous lines, close to the ingot surfaces, are called A-segregates in which the solute is enriched. We can note that the general segregation pattern in the experiment is well reproduced in the simulation, such as top positive segregation, bottom negative segregation, and A-segregates.

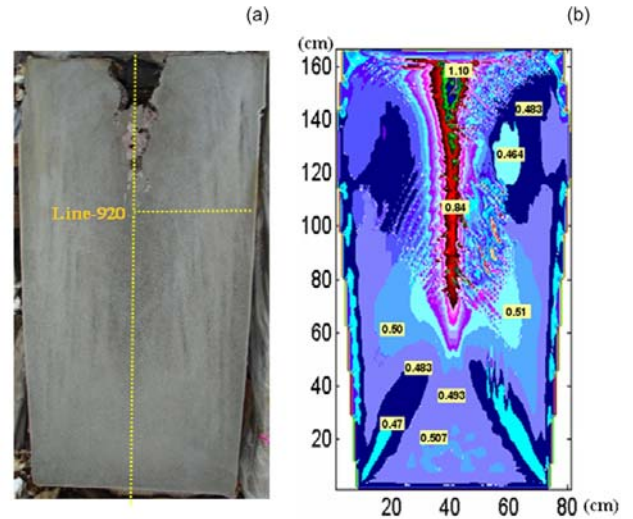


Fig. 5. Carbon segregation map: (a) sulfur-print of the experimental ingot, (b) simulation result.

In Fig. 6a, a fair agreement is noteworthy between experimental measurements and numerical data. However, in Fig. 6b, some apparent discrepancies are present. The oscillating concentration profile is shifted upward in the simulation. The major reason is the solidification shrinkage is not included in the calculation. The height of the bottom negative-segregation cone is well predicted, but the extent of segregation is numerically underestimated due to the neglecting of grain settlement. There is a special phenomenon which needs our attention. At the ingot bottom, both experiment and calculation show a concentration fluctuation (negative-positive-negative pattern). This is against people’s expectation: positive segregation should not exist at the bottom due to the settling of grains. This phenomenon will be analyzed in Section 4.2.

All in all, fair agreements of present simulation

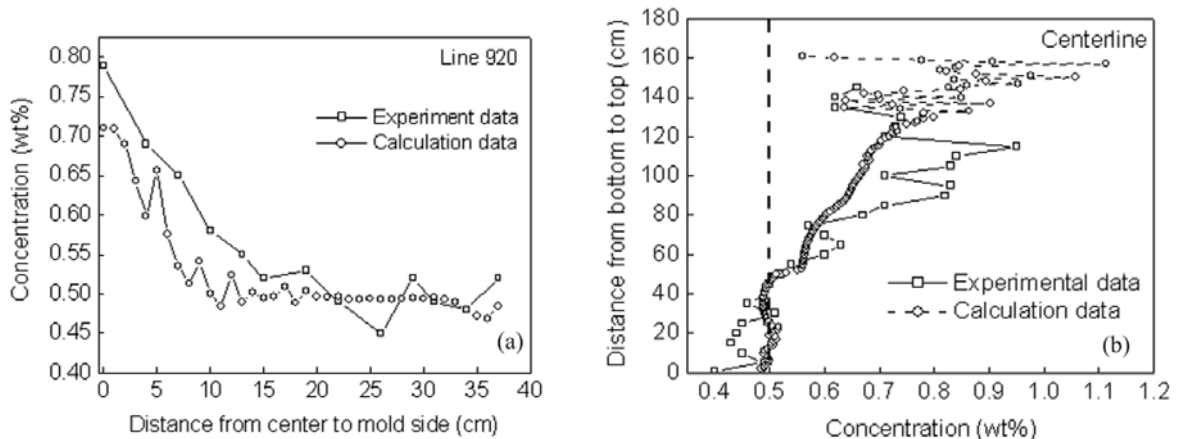


Fig. 6. Segregation in carbon of the ingot: experimental and model results: (a) along line-920, (b) along centerline.

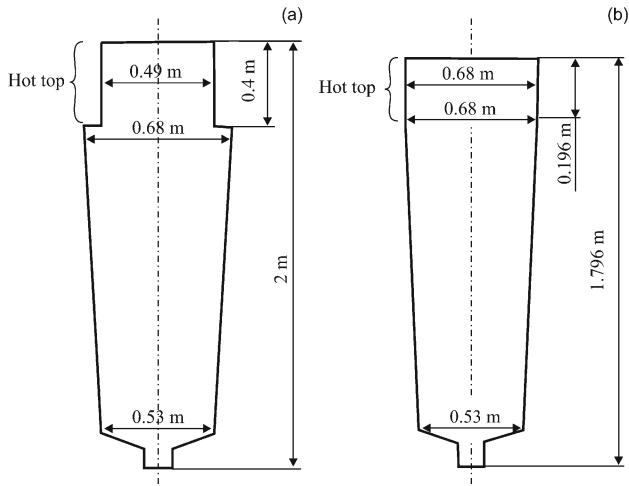


Fig. 7. Schematic diagram of modified ingots: (a) case-1, (b) case-2.

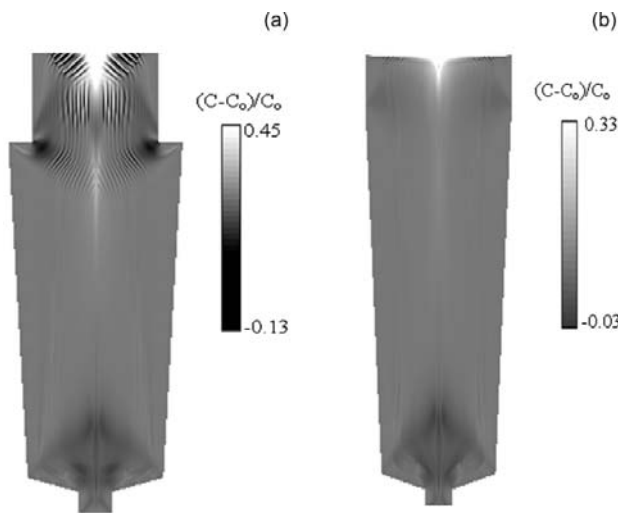


Fig. 8. Carbon segregation ratio map in ingots: (a) case-1, (b) case-2.

with data both in the literature and the experimental measurement confirm that the developed scheme can give a reasonable depiction of physical situation and can be safely used in the following studies.

4. Numerical results and discussion

4.1. Influence of mold shape

In this section, the mold shape in Fig. 1 (base case) is changed. Two modifications are made, as shown in Fig. 7.

Figure 7a: case-1 has the same weight as that of base case, but the height of hot top is reduced from 0.6 m to 0.4 m, and the diameter is decreased from 0.536 m to 0.49 m.

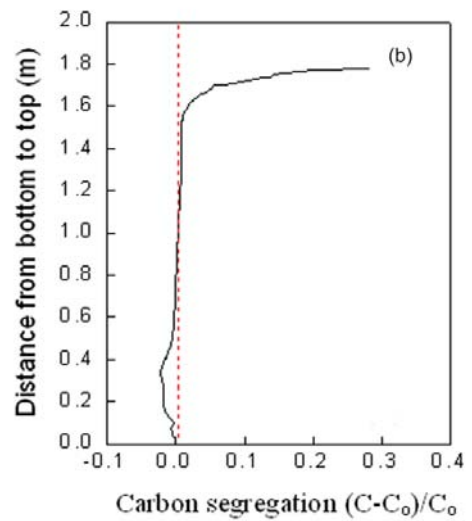
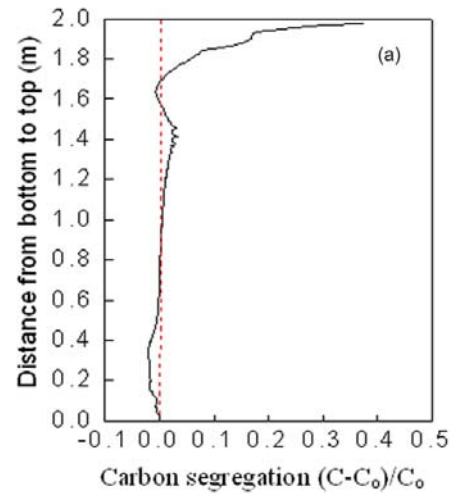


Fig. 9. Carbon segregation distribution along centerline for (a) case-1, (b) case-2.

Figure 7b: case-2 has the same weight as that of base case, but the height of hot top is reduced from 0.6 m to 0.207 m, and the diameter is increased from 0.536 m to 0.68 m. Comparison between case-1 and case-2 shows that only the hot-top shape is changed. The apparent difference is the sharp decrease in the section area for the hot top is avoided in case-2.

Numerical predictions of carbon segregation map for the two cases are shown in Fig. 8, with melt superheat 0°C.

Case-1 (Fig. 8a) presents a similar tendency of macrosegregation to the base case, except that there is a more obvious positive-negative-positive carbon distribution along central axis (Fig. 9a). This can be explained by examining Fig. 10, where solid fraction distribution close to a “special point” is illustrated. As informed by [2], there is a “special point” on the centerline at the level of hot-top joint, where isotherms from two sides of ingot meet with each other. During

solidification, when this point occurs, the local hydrodynamic resistance is increased. It is not easy for the solute-enriched liquid to be transferred from the position below the point to the top part. Then, since case-1 has a larger size of liquid pool below the special point and a higher value of solid fraction at this point, the finally formed positive segregation becomes stronger.

Case-2 (Fig. 8b) has a different segregation distribution in comparison with case-1 and base case. First, the positive-negative concentration variation along centerline is not observed (Fig. 9b). It is clear that unlike case-1 and base case, the solid fraction contour in case-2 does not present a wavy shape, see Fig. 11c. Moreover, as in Fig. 11c, the fluid flow does not change its direction at the level of hot-top joint, e.g. diverting back to the hot top. This is attributed to the fact that the mold shape does not favor the formation of the “special point”. So, the tendency of negative segregation formation is minimized.

Second, in case-2, the local negative segregation is less serious at the joint position of hot-top and ingot body. From Fig. 12 it is seen that since there is no sharp variation in section area from ingot body to hop

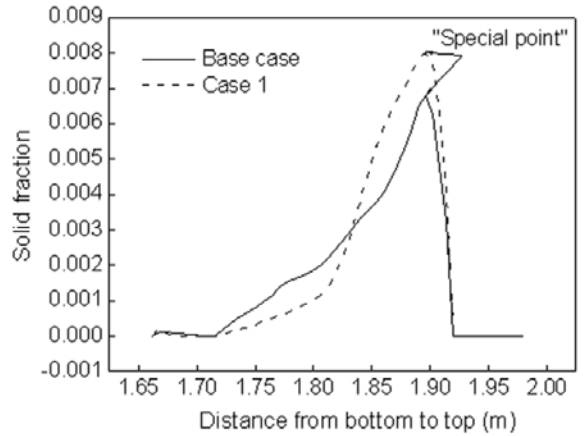


Fig. 10. Solid fraction distribution close to the special point along centerline at 5000 s for base case and case-1.

top, the direction of fluid flow does not change greatly at the joint position. On the contrary, for case-1 and base case, the fluid flow diverts nearly ninety degrees to adapt to the solid fraction contour, which carries a large amount of enriched liquid out of the mush. Then,

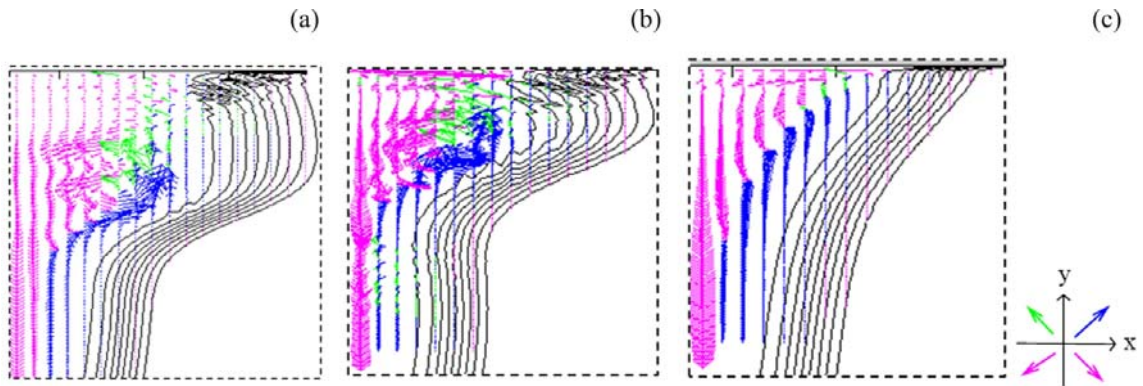


Fig. 11. Flow vectors at the level of hot-top joint at 5000 s for (a) base case, (b) case-1, (c) case-2. Black lines are solid fraction contours.

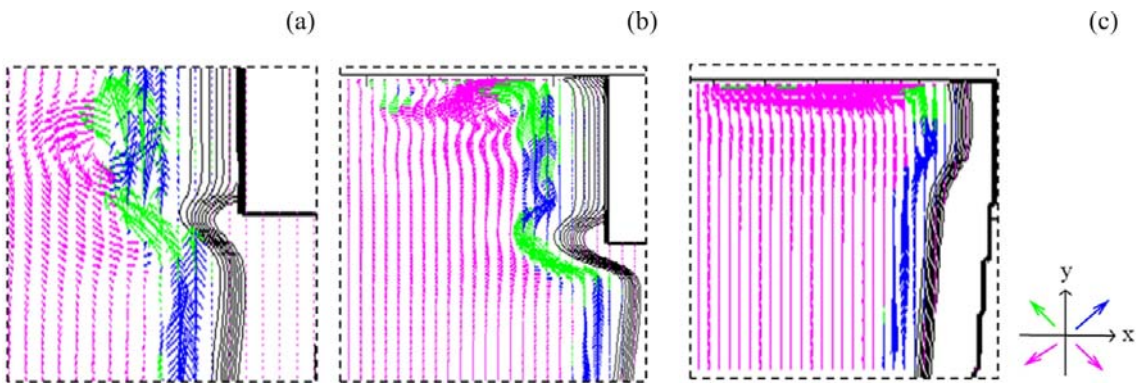


Fig. 12. Flow vectors at the level of hot-top joint at 500 s for (a) base case, (b) case-1, (c) case-2. Black lines are solid fraction contours.

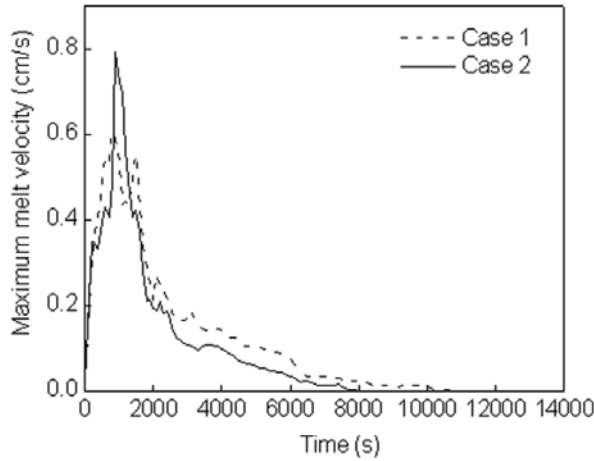


Fig. 13. Maximum melt velocity during solidification for case-1 and case-2.

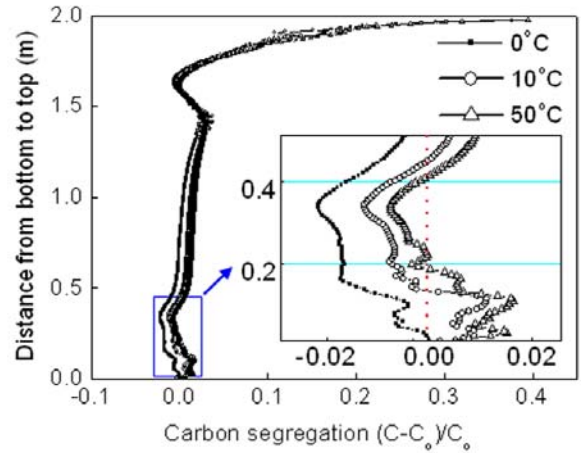


Fig. 15. Carbon segregation distribution along centerline for various superheats.

the solute depletion is more pronounced in case-1 and base case than in case-2.

Third, A-segregates are not found in case-2. On the one hand, the shape of mushy zone does not change abruptly as those in the former two cases. On the other hand, with the lower height and more uniform section area of casting system, the velocity of natural convection becomes weak (see Fig. 13), meaning the degree of disturbance at the solidification front is decreased. As a result, A-segregation is not formed.

4.2. Influence of melt superheat

Case-1 in Section 4.1. is studied. Three melt superheats are selected: 50°C, 10°C and 0°C. Numerical

predictions of carbon segregation ratio map at different superheats are shown in Fig. 14.

For the three cases, the general segregation pattern is similar: bottom negative segregation cone, top positive segregation, and A-segregates. To compare them in a quantitative way, however, Fig. 15 shows some differences.

When the melt superheat is larger than zero, there are concentration fluctuations at the ingot bottom: a small positively-segregated region forms before the negative segregation cone develops. Moreover, the height of bottom negative segregation cone is decreased. All these are mainly ascribed to the variations of flow field induced by superheat. Figure 16 shows the flow field at different times during solidification.

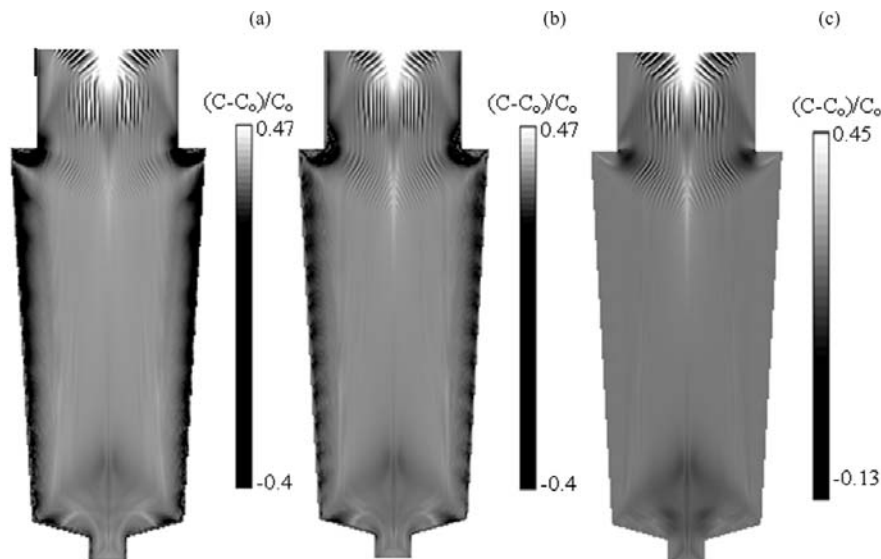


Fig. 14. Segregation ratio map in ingot (case-1) for different melt superheats: (a) 50°C, (b) 10°C, (c) 0°C.

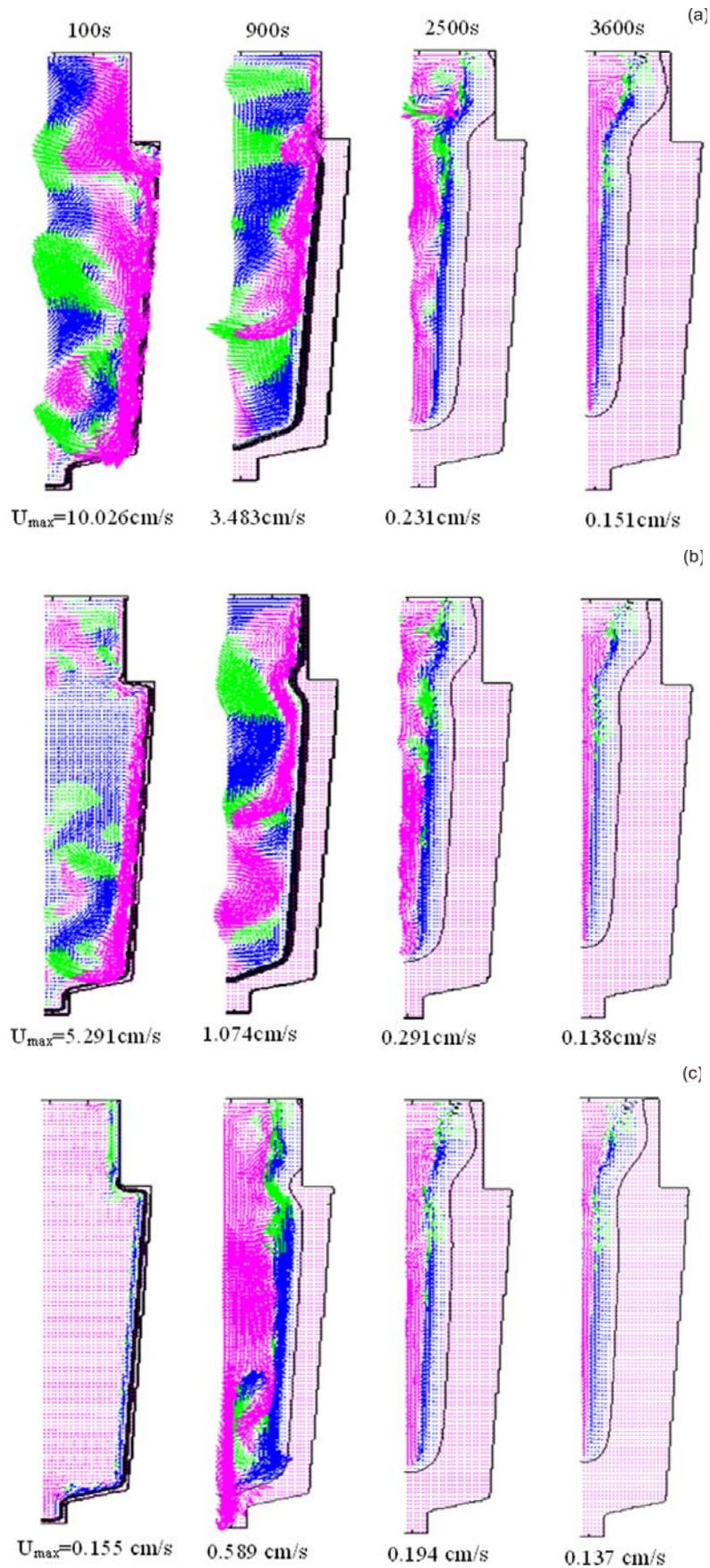


Fig. 16. Flow vectors at various times for different melt superheats: (a) 50°C, (b) 10°C, (c) 0°C. Black lines are solid fraction contours.

Superimposed on the vector plots are solid fraction contours.

At the early stage of solidification (100 s), flow fields are complex for superheats 50°C and 10°C: clockwise and counterclockwise cells coexist in the bulk liquid. According to equation $\frac{\partial C}{\partial t} = -\frac{1}{m_1} f_1 \vec{v}_1 \cdot \nabla T$ in [2], if the temperature gradient has the same direction as that of flow vector, the formation of positive segregation is favored. Or else, negative segregation is formed. Since several flow cells counteract with each other before solutal buoyancy dominates, temperature gradient and flow vector may have the same direction at some position, and then, positive segregation patches occur. However, this phenomenon is not observed for superheat 0°C. At the initial period, a counterclockwise cell exists. Therefore, the possibility that enriched liquid is captured at the bottom due to the destabilized flow is reduced.

At 900 s, for superheats 50°C and 10°C, flow field is still destabilized. Clockwise cells create a flow in the direction of temperature gradient in the center, resulting in the accumulation of solute-rich liquid. So, the height of bottom negative segregation cone is reduced. For superheat 0°C, liquid flows downward in the center and turns upward in the mush. Such a flow pattern favors the development of negative segregation at the ingot bottom. Although a small clockwise cell is noted, it is responsible for the formation of solute-rich patches close to the ingot surface, and has no effect on the formation of bottom negative segregation cone.

At 2500 s, 3600 s and until the end of solidification, the three cases present similar flow fields and solid fraction contours. This guarantees that each case has the top positive segregation, A-segregates and positive-negative-positive segregation distribution along central axis in the final macrosegregation map.

In this paper, although the simulation with superheat = 0°C can only be performed on a numerical research basis, it highlights that the occurrence of positive segregation at the ingot bottom is mainly due to the destabilized fluid flow created by melt superheat during the early stage of solidification. The phenomenon in *Section 3.2* is explained by the above simulation and analysis.

6. Conclusions

Impacts of mold shape and melt superheat on macrosegregation formation of Fe-0.36wt.%C alloy in a 3.3 t ingot are numerically investigated. For the intended use of the self-developed code, the numerical scheme is tested by reproducing the data both in the literature and in the experiment. An acceptable outcome is obtained. Some important findings are summarized as follows:

1. It is shown that with a sharp decrease of section area at the level of hot top joint, a distribution of positive-negative-positive concentration along the centerline is favored. For ingots with the same weight, by decreasing the height of hot top to some extent, a more pronounced positive-negative-positive concentration pattern occurs.

2. If the mold shape is modified to have more uniform section area, the occurrence of positive-negative-positive segregation pattern along the central axis is not noted. Moreover, A-segregates do not occur since the shape of mushy region changes and flow velocity decreases.

3. As the superheat is increased from 0°C to 50°C, the height of bottom negative segregation cone is reduced. With superheat larger than 0°C, the occurrence of positive segregation patches at the ingot bottom is explained as: the solute-enriched liquid is easily to be captured at the bottom region due to the destabilized flow at the initial period of solidification created by melt superheat.

Modeling of macrosegregation formation allows the relative importance of different physical processes on the final segregation pattern to be predicted, and hence, indicates which aspect of the process needs additional effort and experimental research to improve the final product.

Acknowledgements

Authors gratefully acknowledge the financial supports from the “High-end CNC machine tools and basic manufacturing equipment” Major Science and Technology Project of China (No. 2009ZX04014-081), and the Post-Doctor Project of China (No. 20080431162).

References

- [1] GU, J. P.—BECKERMANN, C.: Metall. Mater. Trans. A, 30, 1999, p. 1357. [doi:10.1007/s11661-999-0284-5](https://doi.org/10.1007/s11661-999-0284-5)
- [2] COMBEAU, H.—ZALOZNIK, M.—HANS, S.—RICHY, P. E.: Metall. Mater. Trans. B, 40, 2009, p. 289. [doi:10.1007/s11663-008-9178-y](https://doi.org/10.1007/s11663-008-9178-y)
- [3] LESOULT, G.: Mater. Sci. Eng. A, 413–414, 2005, p. 19. [doi:10.1016/j.msea.2005.08.203](https://doi.org/10.1016/j.msea.2005.08.203)
- [4] SCHNEIDER, M. C.—BECKERMANN, C.: Metall. Mater. Trans. A, 26, 1995, p. 2373. [doi:10.1007/BF02671251](https://doi.org/10.1007/BF02671251)
- [5] RADY, M. A.—SATYAMURTY, V. V.—MOHANTY, A. K.: Metall. Mater. Trans. B, 28, 1997, p. 943. [doi:10.1007/s11663-997-0022-6](https://doi.org/10.1007/s11663-997-0022-6)
- [6] LEE, J. H.—LEE, K.—MOK, J. H.: ISIJ Int., 45, 2005, p. 1151. [doi:10.2355/isijinternational.45.1151](https://doi.org/10.2355/isijinternational.45.1151)
- [7] YADAV, A.—PATHAK, N.—KUMAR, A.—DUTTA, P.—SARKAR, S.: Modelling Simul. Mater. Sci. Eng., 17, 2009, p. 1.

- [8] SANG, B. G.: [PhD Dissertation]. Shenyang, China, Institute of Metal Research 2010.
- [9] VOLLER, V. R.—MOUCHMOV, A.—CROSS, M.: Appl. Math. Model., 28, 2004, p. 79.
[doi:10.1016/S0307-904X\(03\)00115-X](https://doi.org/10.1016/S0307-904X(03)00115-X)
- [10] PARDESHI, R.—VOLLER, V. R.—SINGH, A. K.—DUTTA, P.: Int. J. Heat Mass Transfer, 51, 2008, p. 3401.